Vortex and Strain Skeletons in Eulerian and Lagrangian Frames

Jan Sahner, Tino Weinkauf, Nathalie Teuber, and Hans-Christian Hege, *Member, IEEE,*

***Abstract*— We present an approach to analyze mixing in flow fields by extracting vortex and strain features as extremal structures of derived scalar quantities that satisfy a duality property: they indicate vortical as well as high-strain (saddle-type) regions. Specifically, we consider the Okubo-Weiss criterion and the recently introduced $\mathrm{M_Z}$-criterion. While the first is derived from a purely Eulerian framework, the latter is based on Lagrangian considerations. In both cases high values indicate vortex activity whereas low values indicate regions of high strain. By considering the extremal features of those quantities, we define the notions of a vortex and a strain skeleton in a hierarchical manner: the collection of maximal 0D, 1D and 2D structures assemble the vortex skeleton; the minimal structures identify the strain skeleton. We extract those features using scalar field topology and apply our method to a number of steady and unsteady 3D flow fields.**

***Index Terms*— flow visualization, feature extraction, vortex core lines, strain features**

I. Introduction

Recent advances in time-dependent flow simulations have increased the size of data significantly. Additionally scientists aim at understanding the high dimensional parameter space that governs the flow – geometry optimization as well as active flow actuation are areas in which high degrees of freedom must be controlled. Automatic extraction and quantification of the features of interest are key ingredients to understanding the impact of parameter changes that can finally lead to optimized flow.

The extraction of features as well defined geometric objects is a prerequisite for distance measurements and extent quantification. In this paper, we present an approach for extraction of both vortex and strain features as points, lines and surfaces. The existence of vortices on the one hand and high-strain regions on the other hand drives mixing in a flow. Hence, our techniques can be used as a tool for mixing analysis in flow fields.

For vortex features much research has aimed at extracting lines denoting the core of a vortex: Sujudi et al. [22] extracted lines around which swirling motion of stream lines occurs, Roth et al. [16] described a higher order method. Banks et al. integrated vorticity lines from critical points in the flow [1], correcting towards pressure minima. Stegmaier et al. [20] took a similar approach and suggested to correct towards minima of λ_2. Peikert et al. [15] provided the parallel vectors operator, a framework for vortex core line extraction covering all those methods. Theisel et al. [23] coupled the parallel vectors approach and the feature flow fields approach [24] to track vortex core lines in time. Wiebel et al. [28] developed the localized flow approach which can also be used for Galilean invariant vortex core line extraction. Miura et al. [13] extracted minimum lines of pressure. Sahner et al. [17] extracted vortex core lines as extremum lines of vortex region quantities like λ_2 [11] and Q [10] in a Galilean invariant way. This means, the extracted features are invariant under Galilean changes of the reference frames.

All those approaches aim at the extraction of one dimensional vortex features. In this work, we extend the two latter works by extracting zero-, one- and two-dimensional extremal vortex features as the vortex skeleton, see Figure 2 for a motivating example.

On the other hand, little is known about the extraction of features that can be identified with mixing properties of the flow. Mixing is actively researched in many fields, for instance in burning chambers where fuel and oxygen injection has to be synchronized for optimal combustion. Vector field topology – introduced to the visualization community by Helman et al. [9] – can be used for mixing detection, as saddle points are indicators for strain in the flow, as well as boundary switch and saddle connectors extracted by Theisel and Weinkauf [25], [26]. These are the intersection lines of 2D separatrices showing between which saddles and boundary regions particle transport takes place. Topological methods based on the flow field itself are not Galilean invariant, a property that in many cases is considered necessary from the physical point of view.

In this paper we identify specific, derived scalar quantities of the flow that have a duality property: they detect vortex and strain regions simultaneously. By extracting extremal points, lines and surfaces of those properties we achieve Galilean invariant strain features that together assemble the strain skeleton. With those extracted features at hand we aim at tracking and comparing those structures in the future. However, this is beyond the scope of the this paper. We concentrate on the mere extraction and do not address possibilities of post processing the extracted structures.

This paper is organized as follows: In section II we clarify the notion of dual vortex and strain quantities and identify two criteria that meet this requirement. In section III we define vortex and strain skeletons as the collection of certain extremal structures of these quantities. We show how separation properties can be utilized to quantify the extent of vortex and strin features. Implementation issues of the extremal extraction are given in section IV. Finally, we apply our methods to a number of steady and unsteady data sets in section V before drawing

Manuscript received March 31, 2006; revised October 23, 2006.

All authors are with the Zuse Institute Berlin (ZIB), E-mail: {sahner, weinkauf, teuber, hege}@zib.de

conclusions in section VI.

II. Dual Vortex and Strain Quantities

The most widely used vortex region quantities are based on a decomposition of the flow field gradient $\nabla v = \mathbf{S} + \Omega$ into its symmetric part, the strain tensor

$$\mathbf{S} = \frac{1}{2}(\nabla v + \nabla v^t) \tag{1}$$

and its antisymmetric part, the vorticity tensor

$$\Omega = \frac{1}{2}(\nabla v - \nabla v^t) = \begin{pmatrix} 0 & -\omega_3 & \omega_2 \\ \omega_3 & 0 & -\omega_1 \\ -\omega_2 & \omega_1 & 0 \end{pmatrix}, \tag{2}$$

where $\omega = (\omega_1, \omega_2, \omega_3) = \nabla \times v$ denotes the vorticity. While Ω assesses vortical activity, the strain tensor $\mathbf{S}$ measures the amount of stretching and folding which drives mixing to occur. To motivate the latter, some words are necessary on perturbation advection: in a time dependent flow field consider the path line $x(t; x_0)$ started at x_0 defined by $\dot{x}(t; x_0) = v(x(t; x_0), t)$ and initial condition $x(t_0, x_0) = x_0$. Comparing x to $\tilde{x}(t, \tilde{x}_0)$ with $\tilde{x}_0$ being an infinitesimal perturbation of x_0, the propagated perturbation $\xi(t) = \tilde{x}(t, \tilde{x}_0) - x(t, x_0)$ is gouverned by the linearized dynamical system

$$\dot{\xi} = \nabla v(x(t; x_0), t)\xi, \tag{3}$$

see e.g. [6]. The strain tensor now gives the answer to the question, how the magnitude of the perturbation $|\xi|$ evolves in time when both initial conditions are advected by the flow. This evolution is described by the Lyapunov function

$$V(\xi, t) := \frac{1}{2}\frac{\mathrm{d}}{\mathrm{dt}}|\xi|^2 = \langle \xi, \dot{\xi} \rangle = \langle \xi, \nabla v \xi \rangle = \langle \xi, \mathbf{S}\xi \rangle, \tag{4}$$

where (3) was used as well as the fact that the symmetric scalar product $\langle \cdot, \cdot \rangle$ only sees the symmetric part of ∇v. Where $V < 0$, initial perturbations decay over time, while $V > 0$ indicates their growing. Where perturbations decay or grow drastically the flow exhibits a saddle like pattern – a pattern that drives mixing of fluid particles. Now the Euclidean matrix norm $\|\mathbf{S}\|$, called the rate of strain, supplies a measure for this initial perturbation evolution due to

$$|V(\xi, t)| = |\langle \xi, \mathbf{S}\xi \rangle| \leq |\xi|^2 \|\mathbf{S}\|. \tag{5}$$

Note that although the initial perturbation analysis uses path lines, the quantity $\mathbf{S}$ that measures the perturbation growth is completely Eulerian – it is built out of quantities in a specific snapshot of time.

Inherent to the decomposition of the flow field gradient ∇v into $\mathbf{S}$ and Ω is the following duality: vortical activity is high in regions where Ω dominates $\mathbf{S}$, whereas strain is characterized by $\mathbf{S}$ dominating Ω.

In order to identify vortical activity, Jeong et al. used this decomposition in [11] to the vortex region quantity λ_2 as the second largest eigenvalue of the symmetric tensor $\mathbf{S}^2 + \Omega^2$. Vortex regions are identified by $\lambda_2 < 0$, whereas $\lambda_2 > 0$ lacks physical interpretation. λ_2 does not capture stretching and folding of fluid particles and hence does not capture the vorticity-strain duality detailed above.

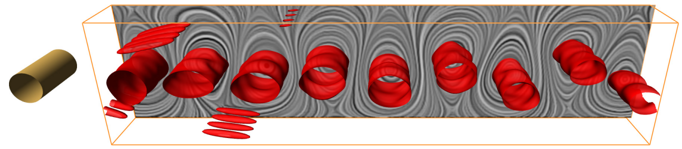

Fig. 1. Isosurfaces of Q showing Eulerian vortex regions in a flow behind a circular cylinder. The LIC-plane is indicating corresponding vortical streamline patterns in the reference frame relative moving with the convection velocity. Throughout the paper, vortex features are colored red, whereas strain features are colored blue.

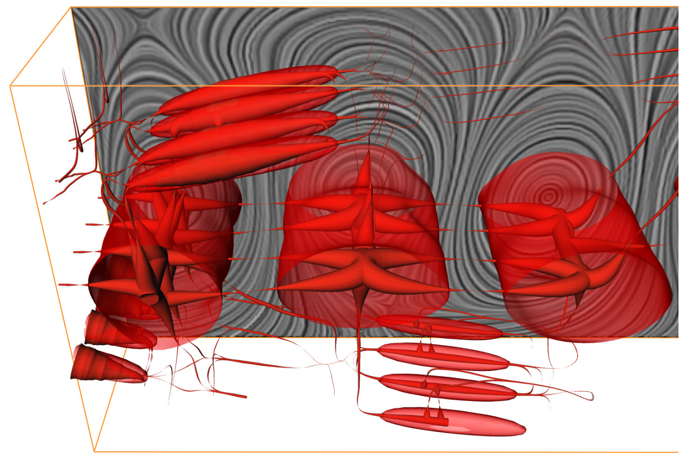

Fig. 2. A closeup of the cylinder dataset showing vortex regions with transparent isosurfaces of Q. This paper aims at extracting 1d and 2d extrema of duality quantities like Q. The lines shown here are the maximum lines of Q where $Q > 0$ extracted by our methods. The lines are scaled by their Q-value and can be regarded as centers of isosurfaces. The correspondence of the lines in the center of the swirling motion shown in the LIC plane justifies the notion of vortex core lines.

In the following subsections we discuss two quantities which utilize the decomposition of ∇v to identify not only vortices but also strain regions. This *duality property* of those quantities will later be used in section III to define 0D, 1D and 2D vortex and strain features that together assemble the corresponding feature skeletons.

A. The Okubo-Weiss Criterion

The Q-criterion of Hunt [10], also known as the Okubo-Weiss criterion, is defined by

$$Q := \frac{1}{2}(\|\Omega\|^2 - \|\mathbf{S}\|^2) = \|\omega\|^2 - \frac{1}{2}\|\mathbf{S}\|^2. \tag{6}$$

Where Q is positive, the vorticity magnitude dominates the rate of strain. Hence it is natural to define vortex regions as regions where $Q > 0$. Unlike λ_2, Q has a physical meaning also where $Q < 0$. Here the rate of strain dominates the vorticity magnitude. The Q-criterion is an Eulerian quantity. Figure 1 shows isosurfaces of $Q > 0$ behind a circular cylinder indicating vortex features. In this figure and throughout the paper, we use red colors to denote vortex features. Blue color will stand for strain features. The data set was derived by Bernd R. Noack (TU Berlin) from a direct numerical Navier Stokes simulation by Gerd Mutschke (FZ Rossendorf). It is a 3D time-dependent Galerkin approximation in the time range $[0, 2\pi]$. It will be explained in detail in section V. We

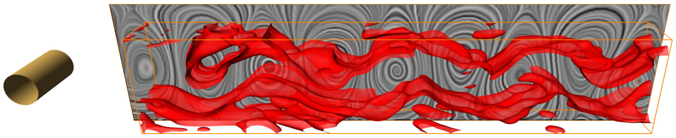

Fig. 3. Isosurfaces of $\mathbf{M_Z}$ showing Lagrangian vortex regions only displayed where path lines could be integrated for 2 seconds.

use this data set throughout the next sections to illustrate our techniques. Figure 1 additionally contains a LIC plane which shows rotational stream line behavior in the frame of reference corresponding to the convection velocity. The isosurfaces correspond to the circular pattern shown in the LIC plane. Note however that Q is a Galilean invariant quantity which is independent of such translational changes of the reference frame.

B. The $\mathbf{M_Z}$-Criterion

Haller has recently proposed the $\mathbf{M_Z}$-criterion that also discriminates vortex and strain regions in incompressible flows similar to the Q-criterion, but in contrast to this based on a Lagrangian analysis [7]. Figure 3 gives an example. To the best of our knowledge the $\mathbf{M_Z}$-criterion has not been used before in 3D-visualization of flow fields. As both the underlying theory and the implementation are quite involved, we give a deeper introduction here.

The $\mathbf{M_Z}$-criterion is based on a strain analysis along path lines. Loosely spoken, Haller proves that path lines along which the strain acceleration tensor M (the tensor describing the first time derivative of V as defined in equation (4)) is positive definite are of saddle type – so called *hyperbolic* lines of maximal strain. In contrast he defines vortices as path lines along which M is indefinite. Such structures are called *elliptic*.

More precisely, Haller argues that in incompressible flows, the function V takes both positive and negative values, as $\mathbf{S}$ has at least one negative and one positive eigenvalue. Hence, the set

$$Z = \{\xi | \langle \xi, \mathbf{S}(x(t),t)\xi \rangle = 0\} \tag{7}$$

is never empty and usually a two dimensional surface, as it separates the regions $V < 0$ and $V > 0$. Physically, within Z, initial bifurcations do not change their magnitude. Hence within Z, the bifurcation evolution is gouverned by the first time derivative

$$\frac{\mathrm{d}}{\mathrm{dt}} V(\xi(t), t). \tag{8}$$

Haller proves that path lines for which $\frac{\mathrm{d}}{\mathrm{dt}}V$ is positive for ξ in Z for all times are of saddle type in the sense that they form stable and unstable manifolds that drive advective mixing in the fluid.

To be able to decide this positivity, we state that

$$\begin{aligned}
\frac{\mathrm{d}}{\mathrm{dt}} V(\xi(t), t) &= \frac{\mathrm{d}}{\mathrm{dt}} \langle \xi(t), \mathbf{S}(x(t),t)\xi(t) \rangle \\
&= \langle \dot{\xi}, \mathbf{S}(x(t),t)\xi \rangle + \langle \xi, \frac{\mathrm{d}}{\mathrm{dt}}(\mathbf{S}(x(t),t)\xi) \rangle \\
&= \langle \nabla v(x(t),t)\xi, \mathbf{S}(x(t),t)\xi \rangle \\
&\quad + \langle \xi, \frac{\mathrm{d}}{\mathrm{dt}}(\mathbf{S}(x(t),t))\xi + \mathbf{S}(x(t),t)\dot{\xi} \rangle
\end{aligned}$$

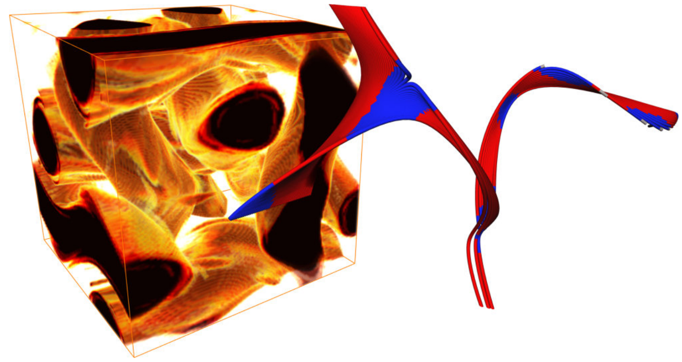

Fig. 4. $\mathbf{M_Z}$-criterion of the periodic ABC-flow. Darker colors indicate higher ellipticity times. Some path lines used for computing $\mathbf{M_Z}$ are shown: hyperbolic points are colored blue, elliptic points are red.

$$\begin{aligned}
&= \langle \xi, (\nabla v^t \mathbf{S} + \frac{\mathrm{d}}{\mathrm{dt}}(\mathbf{S}(x(t),t)) + \mathbf{S}\nabla v)\xi \rangle \\
&= \langle \xi, M\xi \rangle
\end{aligned} \tag{9}$$

where the strain acceleration tensor M is defined as

$$M = \nabla v^t \mathbf{S} + \frac{\mathrm{d}}{\mathrm{dt}}(\mathbf{S}(x(t),t)) + \mathbf{S}\nabla v. \tag{10}$$

The $\mathbf{M_Z}$-criterion is now defined as follows:

Definition 1: $\mathbf{M_Z}$***-criterion - total ellipticity time*** Let (x_0, t_0) be an arbitrary point in the space-time domain of the flow and $x(t)$ the path line with $x(t_0) = x_0$.

1) A point on the path line is called *hyperbolic*, if $\langle \xi, M\xi \rangle$ is positive for all ξ in Z at that point. Physically, such a point describes a saddle type or strain point. Otherwise, the point on the path line is called *elliptic* and indicates vortex behavior.
2) $\mathbf{M_Z}(x_0, t_0)$ is defined as the sum of the lengths of all time intervals, in which the path line started at (x_0, t_0) is elliptic.

Where $\mathbf{M_Z} = 0$, the path lines are hyperbolic for all times, and hence form stable or unstable manifolds as described above. In contrast, where $\mathbf{M_Z}$ equals the integration time of the path lines, maximal vortex activity is present. However, in numerical implementations the path line seeding is necessarily sparse. Thus it is unlikely to find a path line that is completely hyperbolic or completely elliptic. But still, a qualitative property holds for the $\mathbf{M_Z}$-criterion computed on a sparse grid:

- The lower $\mathbf{M_Z}$, the more strain is present (the majority of points on the path line are hyperbolic).
- The higher $\mathbf{M_Z}$, the more vortical behavior is present (the majority of points on the path line are elliptic).

This is a duality property similar to the Okubo-Weiss criterion. Note that the duality of vortex and strain activity is intrinsic to the $\mathbf{M_Z}$-criterion, as $\mathbf{M_Z}$ is solely based on a strain analysis. Hence, Haller defines a vortex as *lack of strain*.

While Q is Galilean invariant, Haller states that $\mathbf{M_Z}$ is invariant even under a larger group of frame changes, the objective group.

The computation of $\mathbf{M_Z}$ relies on the computability of the positivity of $\langle \xi, \mathbf{M}\xi \rangle$ on Z. We address the implementation issues next.

C. Implementation of $\mathbf{M_Z}$

For 3D time-dependent flows, the $\mathbf{M_Z}$-criterion defines a 3D time-dependent scalar field which can be computed as follows:

Algorithm 1: At each time step t_i

1) Generate a set of seeding points for path line integration. This may be the original grid at t_i, a subset thereof, or the grid points of a uniform grid defined in a region of interest.
2) Integrate path lines for T_P seconds. We use a 4th-order Runge-Kutta integration with adaptive step size.
3) For each path line $x(t)$ started at seeding point (x_0, t_i)
   a) Decide for each point on the path line if it is elliptic or hyperbolic (Figure 4).
   b) Add up all times where the path line is elliptic and associate this total time value to x_0 at time t_i.

Figure 4 shows a volume rendering of $\mathbf{M_Z}$ of the analytic ABC-flow as used by Haller in [7]. Note how the saddle-like behavior of the path lines corresponds to hyperbolic (blue) points. However, it also shows a drawback of the method, as the path lines might leave the domain in non-analytic fields before the maximum integration time is reached. Further challenges can be seen in finding a suitable seeding set for path line integration and the determination of the maximum integration time T_P. Both aspects are open research issues regarding $\mathbf{M_Z}$.

For an implementation of the above algorithm, the computation of the positivity of $\langle \xi, M\xi \rangle$ on the zero strain cone Z in step 3a remains to be clarified. Haller argues that Z can be described by an elliptic cone using the eigenvectors e_1, e_2, e_3 of the strain tensor $\mathbf{S}$ and its corresponding eigenvalues s_1, s_2, s_3, ordered such that

$$\operatorname{sign} s_1 = \operatorname{sign} s_2 \neq \operatorname{sign} s_3, \qquad |s|_1 \geq |s|_2. \tag{11}$$

Then writing M in strain basis

$$\hat{M} = (e_1\, e_2\, e_3)^t\, M\, (e_1\, e_2\, e_3)\,, \tag{12}$$

due to the symmetry of Z, the positivity of $\langle \xi, M\xi \rangle$ is equivalent to positivity of the one-parameter function

$$\begin{aligned} m(\alpha) \;=\; & \hat{M}_{11} b \cos^2 \alpha + \hat{M}_{22} a \sin^2 \alpha + \hat{M}_{33} ab \\ & + \sqrt{ab}\Big(2\hat{M}_{13}\sqrt{b}\cos\alpha \\ & \quad + 2\hat{M}_{23}\sqrt{a}\sin\alpha + \hat{M}_{12}\sin 2\alpha \Big) \end{aligned} \tag{13}$$

for all $\alpha \in [0, 2\pi]$, where

$$a = -\frac{s_1}{s_3}, \qquad b = 1 - a, \tag{14}$$

see [7] for details. The performance of the positivity check of m on the interval $[0, 2\pi]$ is of crucial importance for the overall performance of the $\mathbf{M_Z}$-computation, as this check has to be performed $dT \cdot nS \cdot nT$ times, where dT is the number of time steps, nS the number of seeds per time step, and nT is the average number of sample points on a path line. We found that checking for zeros of m using bisection combined with a first-order derivative estimation speeds up the computation about 3 times compared to equidistantly spaced sign checks. However, compared to the Eulerian Q-criterion which can be computed in seconds, the Lagrangian approach of the $\mathbf{M_Z}$-criterion is much more time-consuming. For 128^3 seeding points the computation time can be up to two hours per time step on modern hardware.

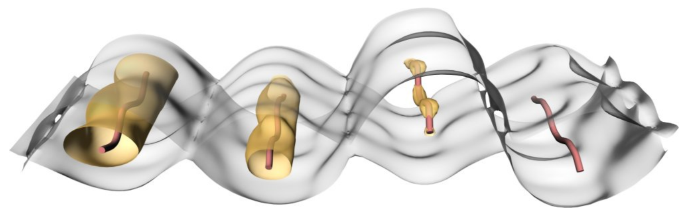

Fig. 5. Isosurfaces are not well suited for higher dimensional extremum extraction: Gray isosurface $Q = 0$ is too far away from strongest vortex activity indicated by the shown extremum lines (red). Yellow isosurface $Q = 2.7$ splits up and misses some regions at all. The maximum lines of Q (red) show location and extent of the vortices correctly.

III. Vortex and Strain Skeletons

This paper aims at the identification of structures of high strain and vortical activity utilizing the criterions discussed in section II. Common parameter-dependent visualization techniques like volume rendering or extraction of isosurfaces are not best suited for this due to the following reasons:

- These approaches require the choice of isovalues or transfer functions, which raises the question of how to choose these parameters appropriately.
- Isosurfaces tend to give wrong answers when it comes to examine the extent of vortices or strain regions since for certain isovalues they split up even inside such regions. For a visualization of the Q-criterion one may choose an isovalue of $Q = 0$ since this separates vortex and strain regions. However, from the resulting visualizations one can usually not infer the regions of strongest activity since typically the surfaces are too far away from those centers (Figure 5).
- Volume rendering is a purely qualitative technique which lacks the availability of sharp geometric features that can be used e.g. to measure distances between vortices.

To avoid these difficulties we choose to extract *extremal* features of Q and $\mathbf{M_Z}$. Due to their duality we identify the following features:

- The 0D, 1D and 2D *minimal* features of those quantities are points, lines and surfaces of maximal strain.
- The 0D, 1D and 2D *maximal* features of those quantities are points, lines and surfaces of maximal vortex activity.

One further property must be regarded for Q: only maximal features for which $Q > 0$ should be regarded as vortical features. On the other hand, only minimal features for which $Q < 0$ should be regarded as strain features. It is not clear if such a natural border exists for the $\mathbf{M_Z}$-criterion. The most natural choice might be $\frac{1}{2}T_P$, the half path line integration time, as there the hyperbolic and elliptic times on the path line balance. However, the actual integration time of each path line may be smaller than T_P since they can leave the domain earlier.

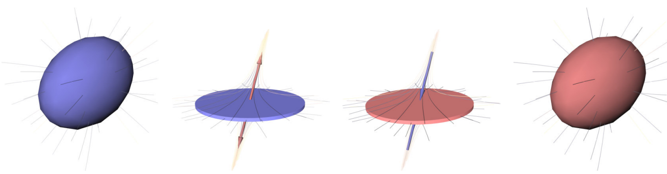

(a) Minimum. (b) Attracting saddle. (c) Repelling saddle. (d) Maximum.

Fig. 6. Classification of critical points in scalar fields.

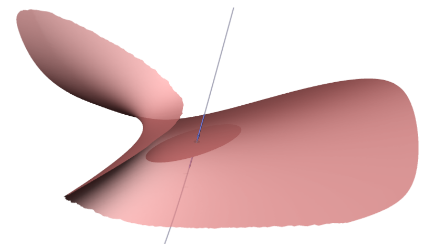

Fig. 7. Separatrices originating from a repelling saddle. The line is a minimal line of steepest descent, the surface is a watershed.

A. Extremal Feature Definition using Scalar Topology

We choose to extract these extremal features using scalar topology. 2D-Scalar topology is closely linked to watershed lines in a 2D-terrain (cf. Figure 10). At certain line structures, rain water separates in the sense that nearby water assembles in different valleys. Those maximum lines partition the domain into valleys. Within valleys all water flows towards the same minimum. Similarly, the domain is partitioned into hills separated by minimal lines called watercourses. On hills all water runs down from one maximum.

The generalization to 3D is straight-forward. Here the watersheds are surfaces, and additional 1D-separatrices come into play. The partitioning of the domain in hills and valleys as well as the corresponding separatrices are the subject of scalar topology. If the scalar function is differentiable, its topology can also be obtained as the vector field topology of its gradient.

The key-elements of scalar topology are so-called critical points, at which the gradient vector field of the scalar function vanishes. Depending on the eigenvalues of the Hessian matrix of the scalar function, those critical points can be classified into four categories (see Figure 6): When all three eigenvalues are positive, the critical point is a minimum, and all gradient lines are leading away from the critical point, so minima are sources (see Figure 6a). A point with exactly one negative eigenvalue is called a repelling saddle (Figure 6c). The unstable manifold emanating from this point has the plane spanned by the eigenvectors corresponding to the positive eigenvalues as its tangent plane. Within this surface, gradient lines lead away from the point. Those surfaces are maximal features, separating minima from each other. We refer to those surfaces as *2D-separatrices*, *maximum surfaces* or *watersheds*. The one-dimensional separatrix tangential to the eigenvector corresponding to the one negative eigenvalue is a minimum line in the scalar field, leading to a minimum following the steepest descent (Figure 7). Those lines are meaningful features, as they can be regarded as centers of isosurfaces, see Figure 5 for an illustrative example and Figure 2 for a real world application. A point with two negative eigenvalues is called attracting saddle (Figure 6b), and its *2D-separartrix* is a *watercourse*, as it separates two maxima from each other. We also refer to the watercourses as *minimum surfaces* [1]. Finally, all eigenvalues are negative at maxima (Figure 6d) and all gradient lines lead into the point, so maxima are sinks.

The utilization of scalar field topology for extremal feature extraction has various advantages: The computation of separatrices as stream lines and stream surfaces of the gradient field is well understood, and stable tools exist for this purpose, see [4], [12] and section IV. No higher than first derivatives of the scalar field are being used, resulting in more stable algorithms as opposed to curvature based methods. Also, recent advances in scalar topology allow topological simplification of three-dimensional scalar fields using the Morse-Smale-Complex [5], answering the question, which topological features are most persistent.

All topological separatrices are of global nature. E.g., it is impossible to decide if a given point lies on a watershed by a local analysis.

By the separation property of watersheds and watercourses, watercourses of Q still have a meaning where $Q > 0$: although they can not be regarded as strain structures there, they still separate two regions of maximal vortex behavior (and analogously for maximal structures where $Q < 0$). By using this separation property of minimum surfaces and neglecting their meaning as a strain structure, we can separate vortex regions from each other, and analogously for strain regions, see Figure 9. Using the notion of watersheds we define

Definition 2: **(Vortex and Strain Skeletons)**

1) The *strain skeleton* is the collection of minima, minimum lines and minimum surfaces of the duality quantities Q (where $Q < 0$) and $\mathbf{M_Z}$. The minimum surfaces partition the flow into vortex domains.
2) The *vortex skeleton* is the collection of maxima, maximum lines and maximum surfaces of the duality quantities Q (where $Q > 0$) and $\mathbf{M_Z}$. Following the notion of [17], lines in the vortex skeleton of Q are Galilean invariant vortex core lines with respect to Q. The maximal surfaces partition the flow into strain domains.

We argue to call the surfaces in the strain skeleton strain surfaces. Accordingly, surfaces in the vortex skeleton are called vortex surfaces as direct generalization of the approach in [17] where Galilean invariant vortex core lines are extracted as extremum lines of vortex region quantities. By intuition, a vortex is a line with spiralling streamlines around it, but this is not necessarily the case for all vortices, see [11].

Figure 8 shows how the vortex and strain skeletons of Q can be used for hierarchical feature display, considering a subregion of the cylinder dataset as an example. Throughout this paper, all strain structures are colored blue. Vortex structures are colored red. In 8a, minima and minimum lines scaled according to the scalar value of Q give a powerful overview of the strain structures, showing the most prominent features in one view. In 8b, the complete strain skeleton is shown. The additionally displayed surfaces show that the lines of extremal

[1] *Minimum surfaces* should not to be mixed up with *Minimal Surfaces*, denoting surfaces of zero mean curvature in mathematics

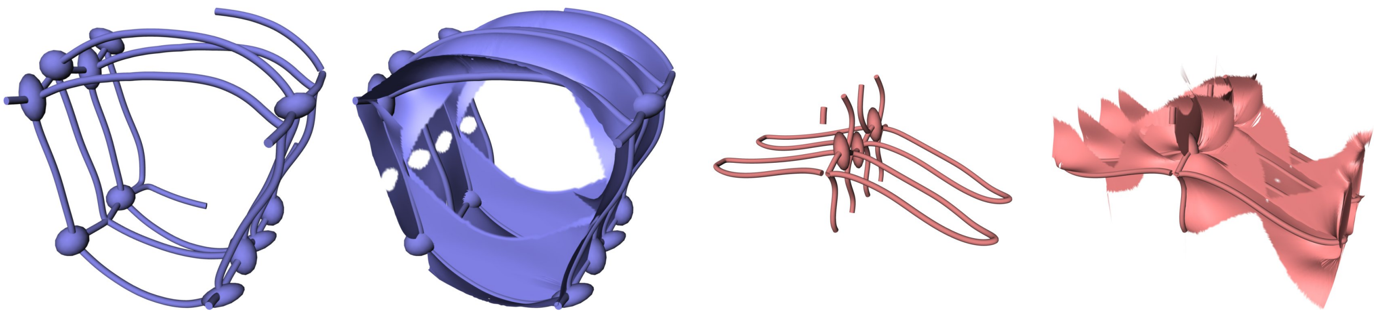

(a) Lines of maximal strain. (b) Strain skeleton. (c) Maximal lines are vortex cores. (d) Vortex skeleton.

Fig. 8. Strain and vortex skeletons in a subregion of the cylinder dataset. 8a shows lines of maximal strain. 8b shows the complete strain skeleton with the extremal strain surfaces displayed only where $Q < 0$. 8c shows the maximal vortex lines regarded as vortex core lines. 8d shows the complete vortex skeleton, adding the maximal vortex surfaces that lie between the vortex core lines. Again, vortex surfaces are displayed only where $Q > 0$.

strain lie inside extremal strain surfaces. Analogously, Figure 8c shows the vortex core lines with respect to Q. The complete vortex skeleton is shown in 8d where the vortex core lines are complemented by the maximum vortex surfaces. Both for the vortex and for the strain skeleton, just those parts of the separatrices are shown where $Q > 0$ and $Q < 0$, respectively.

Figure 9 gives an example where the minimum surfaces are used to subdivide a vortex in further regions. Only parts are shown where $Q < 0$, so an isosurface of $Q = 0$ would label all shown features as belonging to the same vortex. By showing the minimum surfaces (blue) we see how the vortex core line is subdivided into three parts, corresponding to the three maxima of Q along the line.

The extremal structures give a complete overview of the topology of the scalar quantities and hence of the vortex and strain activities in the flow. Note that this includes primary and secondary vortex structures. Primary vortex structures, e.g. Kelvin-Helmholtz vortices, can be observed in the cylinder flow as spanwise vortex core lines (Figure 2) – in this example they correspond to patterns of swirling stream lines in a certain frame of reference. Secondary vortex structures, e.g. rib vortices, are streamwise vortex core lines in the cylinder flow connecting neighboring Kelvin-Helmholtz vortices. This pattern is typical to shear flows and can be observed in other data sets as well (see Section V). Note that secondary vortex structures can not be described as patterns of swirling motion using an obvious frame of reference, i.e., their extraction has to be based on measures independent of a certain reference frame. While our technique is able to extract those features, it does not allow to distinguish between primary and secondary vortices. This is an open research issue.

Before we give details about our extraction scheme in section IV, we motivate our choice of topological separatrices as features.

B. Watersheds vs. Height Ridges

While there is just one reasonable definition for a local 0D-extremum of a scalar quantity f, there is no canonical generalization to higher-dimensional features. Topological separatrices (watersheds and watercourses) are just one choice, see [3] and [18]. Another prominent approach is the height ridge

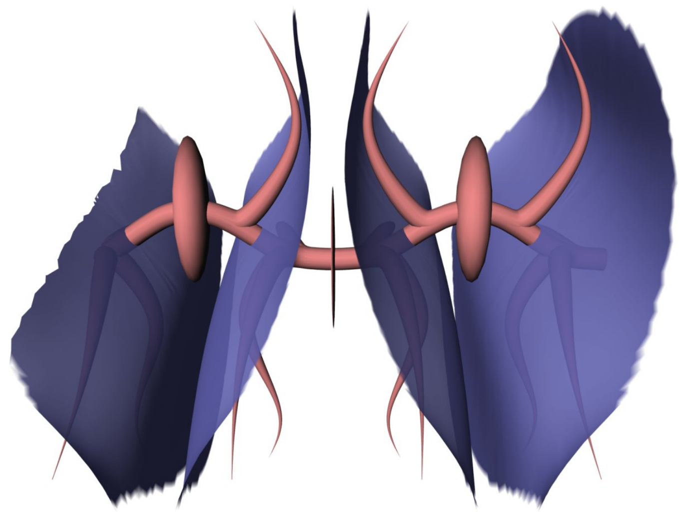

Fig. 9. A close-up of the cylinder dataset. Three maxima of Q (red ellipsoids) are separated from each other by minimum surfaces (blue). This devides the domain into three different vortex regions. The maxima are connected by a maximum line (red), i.e., a vortex core line defined by Q.

definition (see e.g. Eberly [3]) that is based on a convexity-analysis of the graph of f. We give a short introduction here and discuss advantages and disadvantages of both approaches to motivate our choice for the watershed definition. We refer to [3] for a deeper discussion.

Basically, a height ridge line follows the least-convexity-direction of the graph. More formally, a d-dimensional height ridge of a smooth function f with gradient ∇f and Hessian Hf with eigenvalues $\gamma_1 \leq \gamma_2 \leq \gamma_3$ and corresponding eigenvectors c_1, c_2, c_3 is defined as the set of points x where

1) $P_i(x) := \nabla f(x) c_i = 0$ for all $i = 1, \ldots, 3 - d$ and
2) $\gamma_{3-d} < 0$.

d-dimensional height valleys of f are defined as d-dimensional ridges of $-f$. As one expects of such a definition, 0-dimensional height ridges are local maxima.

While implementational details on height ridge extraction can be found in [3], we just sketch the procedure here: $d_r = \nabla P_1 \times \nabla P_2$ is the direction in which a person on a height ridge line can walk along it. Given one point on each height ridge, it is sufficient to integrate d_r from each point to obtain the complete set of height ridges. Accordingly, a two dimensional

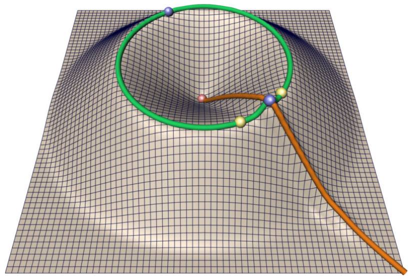

Fig. 10. 2D-terrain exemplifying different extrema definitions. The closed green line is a watershed separatrix. Both the green and the orange line conform to the height ridge definition.

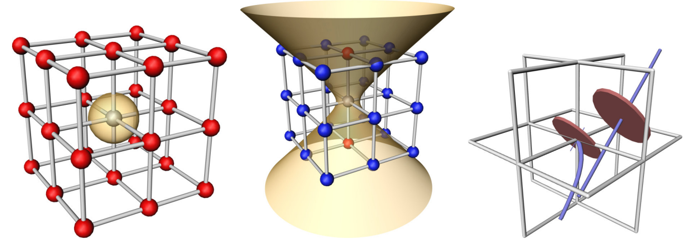

(a) Minimum. (b) Attracting saddle. (c) 1D-separatrix integration.

Fig. 11. Discrete critical point extraction (exemplified using a regular grid). Red nodes are larger than the central node, blue nodes are smaller. Saddles can be extracted by counting the number of connected components of the 26 neighbors (11b). 11c shows that for separatrix integration, the continuously extracted critical points must be used, because the zeros of the gradient do not necessarily lie on grid nodes.

height ridge is given implicitly by the surface normal ∇P_1.

With those two different extrema definitions at hand the question arises, how they are related, and if the features of the one definition are possibly a subset of the other feature set. To this end, we note that at each saddle point with a Hessian matrix of full rank 1) holds for $i = 1, 2, 3$ in the definition of height ridges above. It is a consequence of the inverse function theorem [21] that depending on the eigenvalue setting, either a 2D height ridge and a 1D height valley or a 2D height valley and a 1D height ridge emanates from the saddle point.

So for every topological separatrix there exists a height ridge or valley counterpart. Note that although they have the saddle point in common, they do not necessarily have to coincide.

In contrast, there usually exists a variety of height ridges that are not topological separatrices. Figure 10 gives an example. Here we see a circular watershed on the crater rib, separating the local minimum inside the crater from the global minimum outside the crater. Additionally, a small perturbation of the symmetry of the crater rib creates a height ridge without separation property. This can be regarded as a consequence of the fact that watersheds are of global nature, whereas the definition of height ridges is local.

This locality is the main advantage of the height ridge definition. By this property it is possible to track a height ridge point in time using the feature flow field approach [24], but it is impossible to do so with a point on a watershed – simply due to its global nature. Although the time tracking of extremal features is beyond the scope of this paper, we want to sketch how this disadvantage of topological separatrices can be overcome: As a watershed is always a 2D-separatrix of some saddle, it can be followed in time by tracking the corresponding saddle point first [24], [27] and extracting the separation surface again afterwards.

We see three disadvantages of the height ridge definition for our purposes: Firstly, height ridge extraction is per se less stable than watershed extraction, as the height ridge definition is based on the 2nd derivative of the scalar, and the watershed definition above uses first derivatives only. See Section IV for comments on a discrete, derivative-free implementation. Furthermore, height surface extraction suffers from the additional difficulty that those surfaces are only implicitly defined by the surface normal ∇P_1, and can not be regarded as a stream surface. Finally, we do not know of any persistence considerations for height ridges, as they exist for the topological separatrices using the Morse-Smale-Complex.

IV. Extremal Feature Extraction

In this section we provide implementational details for the extraction of topological features required for the vortex and strain skeletons. We discuss discrete and continuous extraction methods. The provided discrete methods work for arbitrary grids. The continuous versions require an interpolated gradient of the quantities.

A. Critical points

Several numerical methods for *continuous* critical point extraction of the gradient vector field are at hand. In tetrahedral grids, zeros can be computed explicitely [22]. In regular and curvilinear grids, we use a simple subdivision approach: a cell is checked whether one of the three components of the gradient is positive/negative at *all* 8 corners of the cell. If so, no zero is found inside. Otherwise, we recursively subdivide into 8 subcells until their size is smaller than a certain threshold.

A *discrete* method on grids with monotone interpolation works as follows: In this setting, all minima, saddles and maxima necessarily lie on the grid nodes. It clearly can be decided by looking at the direct neighbors, if the point is a minimum or maximum. A saddle point can be decided by labelling the neighbors as *larger* and *smaller* respectively. If more than one connected component exists of any type, the grid node is a saddle, see Figure 11b for a regular grid example.

Note that both approaches result in similar, but not identical sets of critical points. This is due to the fact that common interpolation schemes are not necessarily differentiable, and hence the continuously extracted critical points not necessarily lie on the grid nodes, see Figure 11c.

B. 1D-separatrices

The 1D-separatrices are stream lines of the gradient field by definition, being integrated from saddle points in direction of their eigenvector corresponding to the unique negative or positive eigenvalue, see Figures 6c and 6b. Two seeding points are placed stepping away from the saddle in that eigenvector's direction. Afterwards, a forward integration from those two points yields the separation line for a positive eigenvalue, and

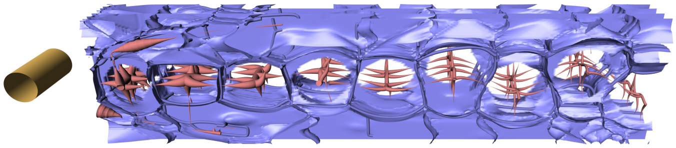

Fig. 12. Strain skeleton of the cylinder data set. It partitions the domain in vortex regions. Inside the vortex regions, lines of maximal vortical behavior are shown scaled by Q. Close-ups of the structures can be seen in Figure 8.

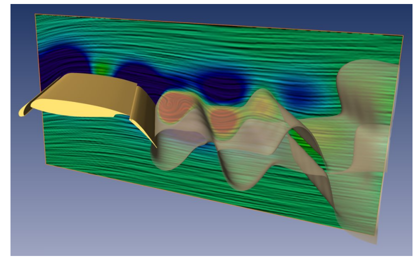

Fig. 13. SCCH airfoil visualized using isosurface $Q = 0$ and a LIC plane colored by Q.

backward for a negative eigenvalue. Note that for the seeding, the continuously extracted critical points must be used. Using the discretely extracted points would cause missing parts of the separatrix, because the two seeding points do not necessarily lie on opposite sides of the critical point(Figure 11c).

Note that (minimum) 1D-separatrices are the lines where the (minimum) 2D-separatrices join in non-manifold junctions, Figure 8. This property can be used for a *discrete* extraction.

C. 2D-separatrices

A *continuous* method for 2D-separatrix extraction is a gradient stream surface integration from saddle points. As a seeding structure, a circle centered at the critical point can be used that lies in the plane spanned by the two eigenvectors of matching sign. From this seeding line a forward or backward stream surface integration is performed, depending on the sign of the eigenvalues. Again, the continuously extracted zeros must be used.

A *discrete* method called the watershed transformation [18] uses the watershed property of 2D-separatrices: Based on the discretely extracted minima, the maximal topological separatrices can be obtained by shedding water in the following way: At start, each minimum gets its own label and is put in a priority queue. Now a region growing is performed. In each step, the unprocessed grid node with the smallest scalar value is grown by one grid node in each direction. The priority queue decides which grid node is processed next. As a result, we obtain a segmentation of the domain by label regions with time complexity $n \log n$. The watersheds can now be extracted as the border surfaces between label regions. We use the generalized marching cubes algorithm for this purpose due to Hege et al. [8].

We use the discrete separation surface extraction as it is faster and more robust.

V. Applications

Figures 1, 3, 5, 8, 9 and 12 show the flow behind a circular cylinder. The data set was derived by Bernd R. Noack (TU Berlin) from a direct numerical Navier Stokes simulation by Gerd Mutschke (FZ Rossendorf). It resolves the so called ‘mode B’ of the 3D cylinder wake at a Reynolds number of 300 and a spanwise wavelength of 1 diameter. The data is provided on a $265 \times 337 \times 65$ curvilinear grid as a low-dimensional Galerkin model [14], [29]. The examined time range is $[0, 2\pi]$. The flow exhibits periodic vortex shedding leading to the well known von Kármán vortex street. This phenomenon plays an important role in many industrial applications, like mixing in heat exchangers or mass flow measurements with vortex counters. However, this vortex shedding can lead to undesirable periodic forces on obstacles, like chimneys, buildings, bridges and submarine towers. Figure 12 shows the complete strain skeleton of the cylinder dataset in blue, partitioning the flow into compartments that correspond to a single vortex each. Inside the compartments, the line structures of the vortex skeleton are shown.

Figures 13 and 14 show the flow around a Swept-Constant-Chord-Half-model (SCCH) of an airfoil that was simulated by Bert Günther (TU Berlin) at a Reynolds number of 10^6 on a curvilinear block structured grid with 1.3 million cells. Due to the constant chord and periodic boundary conditions this is a 2.5D configuration. The sweep angle of the airfoil to the flow direction is $30°$ and the angle of attack is $6°$. The turbulence was simulated by a combined URANS and DES approach. Figure 14b shows the line type structures of the vortex and strain skeletons of Q. Note that by our method, the collection of all extremal strain and vortex lines provide a good overview over the dataset, while the isosurfaces in Figure 14a miss the smaller features downstream.

In Figure 15 we applied our methods to a 3D time-dependent turbulent mixing layer. The velocity field has been computed with a pseudo-spectral direct numerical simulation by Pierre Comte, employing the computational domain and boundary conditions of [2]. The Reynolds number is 100 based on the initial shear-layer thickness and convection velocity. The velocity ratio between the upper and lower stream is $3 : 1$ (Figure 15a). The data consists of 500 time steps of a $480 \times 48 \times 96$ uniform grid. Figure 15b shows the minimum lines of $\mathbf{M_Z}$ which correspond to lines of maximal strain. It can clearly be seen that those structures lie in the shear layer which corresponds to intuition. In 15c isosurfaces of Q display the spatial evolution of Kelvin-Helmholtz vortices (primary vortex structures), vortex pairing, and the spanwise formation of streamwise rib vortices (secondary vortex structures). In 15d the vortex skeleton of Q is shown with lines scaled by the value of Q. The whole vortex structure of the flow can be seen at one view. In particular, our method is capable of resolving secondary vortex structures as well as the less vortical structures further upstream that are hidden by the isosurfaces in 15c.

VI. Conclusions

In this paper we made the following contributions:

- We discussed and clarified the duality of vortex and strain measurement.

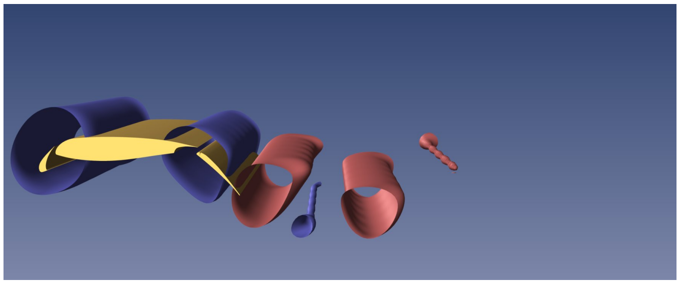

(a) Isosurfaces of $Q < 0$ denoting strain (blue) and $Q > 0$ denoting vortex activity (red).

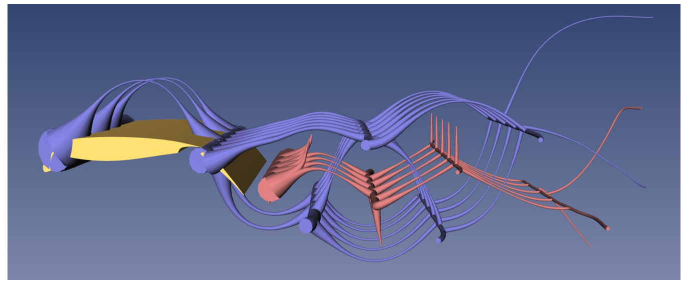

(b) Lines of maximal strain (blue) and maximal vortex activity (red) scaled by $|Q|$.

Fig. 14. In the flow around an airfoil, isosurfaces of the Okubo-Weiss criterion Q are shown to the left. To the right, the line structures in the vortex and strain skeletons extracted by our method are displayed, showing lines of maximal strain (blue) and lines of maximal vortex activity (red) that are vortex core lines. Our method gives a complete overview of the location and extent of vortex and strain features in the flow, whereas the isosurfaces miss the smaller features downstream and give only a rough location for the larger features upstream.

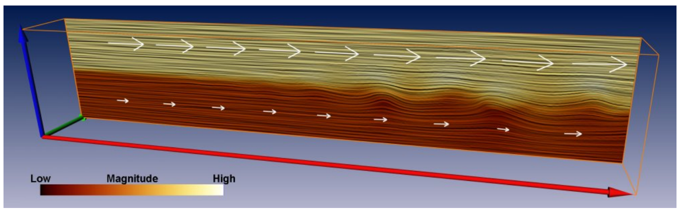

(a) Flow visualized using LIC.

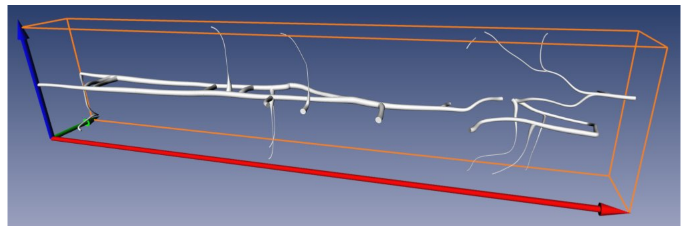

(b) Lines of maximal strain of $\mathbf{M_Z}$.

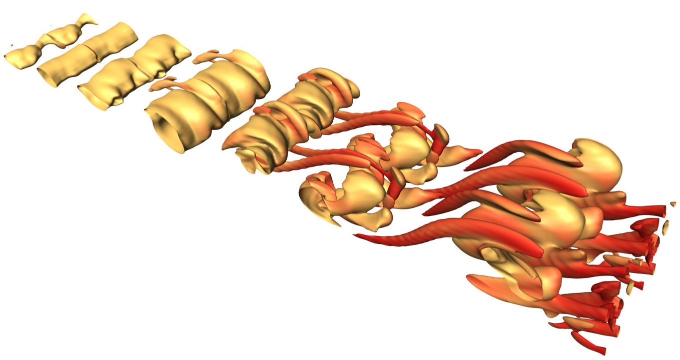

(c) Isosurface of Q.

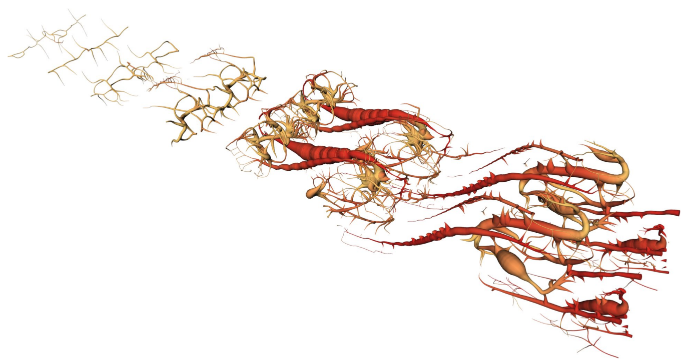

(d) Lines of maximal vortex activity scaled by Q.

Fig. 15. Turbulent mixing layer. The lines of maximal strain as indicated by $\mathbf{M_Z}$ perfectly match up with the shear layer. The vortex skeleton of the Q-criterion elucidates the spatial evolution of Kelvin-Helmholtz vortices, vortex pairing, and the spanwise formation of streamwise rib vortices.

- We extracted Galilean invariant strain features for the first time, resulting in 0D, 1D and 2D features.
- We extracted Galilean invariant vortices including primary and secondary vortex structures.
- We introduced the notion of vortex and strain skeletons. Due to the separation properties of the chosen extraction, we are able to separate vortices as well as strain regions and quantify their extent.

For the future we plan to incorporate topologically persistent simplification to the extracted features. Feature tracking in time is another interesting research topic for the extracted skeletons.

The application to a number of data sets shows the feasibility of our method even for complex settings. We conclude that the visualization of the vortex and strain skeletons support the quantification of both strength and extent of the features in question.

Acknowledgments

We thank Holger Theisel for the constant collaboration. We thank Bernd R. Noack for the fruitful discussions and the supply of the cylinder data set which was kindly provided by Gerd Mutschke (FZ Rossendorf). We thank Bert Günther (airfoil) and Pierre Comte (mixing layer) for providing the data sets. We thank Steffen Prohaska for his sharp thoughts and code. We thank George Haller and Jon Scouten for their thoughtful comments. All visualizations in this paper have been created using AMIRA – a system for advanced visual data analysis [19] (see `http://amira.zib.de/`).

References

[1] D.C. Banks and B.A. Singer. A predictor-corrector technique for visualizing unsteady flow. *IEEE Transactions on Visualization and Computer Graphics*, 1(2):151–163, 1995.

[2] P. Comte, J.H. Silvestrini, and P. Bégou. Streamwise vortices in Large-Eddy Simulations of mixing layer. *Eur. J. Mech. B*, 17:615–637, 1998.

[3] D. Eberly. *Ridges in Image and Data Analysis*. Kluwer Acadamic Publishers, Dordrecht, 1996.

[4] C. Garth, X. Tricoche, T. Salzbrunn, T. Bobach, and G. Scheuermann. Surface techniques for vortex visualization. In *Proc. IEEE TCVG Symposium on Visualization 2004*, pages 155–164, 2004.

[5] A. Gyulassy, V. Natarajan, V. Pascucci, and P.-T. Bremer B. Hamann. Topology-based simplification for feature extraction from 3d scalar fields. In *Proc. IEEE Visualization 2005*, pages 535–542, 2005.

[6] J.K. Hale. *Ordinary Differential Equations*. Kreiger, New York, 1980.

[7] G. Haller. An objective definition of a vortex. *J. Fluid Mech.*, 525:1–26, 2005.

[8] H.-C. Hege, M. Seebass, D. Stalling, and M. Zöckler. A generalized marching cubes algorithm based on non-binary classifications. *Preprint SC-97-05*, 1997. ZIB, Berlin.

[9] J. Helman and L. Hesselink. Representation and display of vector field topology in fluid flow data sets. *IEEE Computer*, 22(8):27–36, August 1989.

[10] J.C.R Hunt. Vorticity and vortex dynamics in complex turbulent flows. *Proc CANCAM, Trans. Can. Soc. Mec. Engrs*, 11:21, 1987.

[11] J. Jeong and F. Hussain. On the identification of a vortex. *J. Fluid Mechanics*, 285:69–94, 1995.

[12] B. Krauskopf, H. M. Osinga, E. J. Doedel, M. E. Henderson, J. M. Guckenheimer, A. Vladimirsky, M. Dellnitz, and O. Junge. A survey of methods for computing (un)stable manifolds of vector fields. *Int. J. Bifurcation & Chaos*, 15(3):763–791, 2005.

[13] H. Miura and S. Kida. Identification of tubular vortices in turbulence. *J. Physical Society of Japan*, 66(5):1331–1334, 1997.

[14] B.R. Noack and H. Eckelmann. A low-dimensional Galerkin method for the three-dimensional flow around a circular cylinder. *Phys. Fluids*, 6:124–143, 1994.

[15] R. Peikert and M. Roth. The parallel vectors operator - a vector field visualization primitive. In *Proc. IEEE Visualization 99*, pages 263–270, 1999.

[16] M. Roth and R. Peikert. A higher-order method for finding vortex core lines. In D. Ebert, H. Hagen, and H. Rushmeier, editors, *Proc. IEEE Visualization '98*, pages 143–150, Los Alamitos, 1998. IEEE Computer Society Press.

[17] J. Sahner, T. Weinkauf, and H.-C. Hege. Galilean invariant extraction and iconic representation of vortex core lines. In *Proc. EuroVis 2005*, pages 151–160, 2005.

[18] Pierre Soille. *Morphological Image Analysis*. Springer, Berlin, Heidelberg, New York, 1999.

[19] D. Stalling, M. Westerhoff, and H.-C. Hege. Amira: A highly interactive system for visual data analysis. *The Visualization Handbook*, pages 749–767, 2005.

[20] S. Stegmaier, U. Rist, and T. Ertl. Opening the Can of Worms: An Exploration Tool for Vortical Flows. In *Proc. IEEE Visualization 05*, pages 463–470. IEEE, 2005.

[21] Robert S. Strichartz. *The Way of Analysis*. Jones & Bartlett Publishers, corr. 3rd printing edition, 1995.

[22] D. Sujudi and R. Haimes. Identification of swirling flow in 3D vector fields. Technical report, Department of Aeronautics and Astronautics, MIT, 1995. AIAA Paper 95-1715.

[23] H. Theisel, J. Sahner, T. Weinkauf, H.-C. Hege, and H.-P. Seidel. Extraction of parallel vector surfaces in 3d time-dependent fields and application to vortex core line tracking. In *Proc. IEEE Visualization 2005*, pages 631–638, 2005.

[24] H. Theisel and H.-P. Seidel. Feature flow fields. In *Data Visualization 2003. Proc. VisSym 03*, pages 141–148, 2003.

[25] H. Theisel, T. Weinkauf, H.-C. Hege, and H.-P. Seidel. Saddle connectors - an approach to visualizing the topological skeleton of complex 3D vector fields. In *Proc. IEEE Visualization 2003*, pages 225–232, 2003.

[26] T. Weinkauf, H. Theisel, H.-C. Hege, and H.-P. Seidel. Boundary switch connectors for topological visualization of complex 3D vector fields. In *Data Visualization 2004. Proc. VisSym 04*, pages 183–192, 2004.

[27] T. Weinkauf, H. Theisel, H.-C. Hege, and H.-P. Seidel. Feature flow fields in out-of-core settings. In *Proc. Topo-In-Vis 2005, Budmerice, Slovakia*, 2005.

[28] Alexander Wiebel, Christoph Garth, and Gerik Scheuermann. Localized flow analysis of 2d and 3d vector fields. In *Proc. EuroVis 2005*, pages 143–150, 2005.

[29] H.-Q. Zhang, U. Fey, B.R. Noack, M. König, and H. Eckelmann. On the transition of the cylinder wake. *Phys. Fluids*, 7(4):779–795, 1995.

Jan Sahner studied mathematics at the Rheinische Friedrich-Wilhelms-University of Bonn, Germany, where he received his M.S. degree in 2003. Since 2004 he has been performing research as a Ph.D. student at the Scientific Visualization department of Zuse Institute Berlin (ZIB). He is associated with the Collaborative Research Center "Control of Complex Turbulent Flows" (Sfb 557), where he works on feature based analysis and comparison techniques for flow fields. His current research interests focus on feature extraction in flow fields.

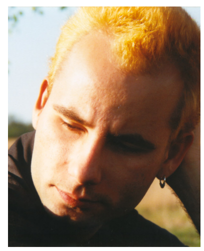

Tino Weinkauf studied computer science with the focus on computer graphics at the University of Rostock, Germany, where he received his M.S. degree in 2000. Since 2001 he has been performing research as a Ph.D. student at the Scientific Visualization department of Zuse Institute Berlin (ZIB). He is associated with the Collaborative Research Center "Control of Complex Turbulent Flows" (Sfb 557), where he works on feature based analysis and comparison techniques for flow fields. His current research interests focus on flow and tensor analysis, information visualization and visualization design.

Nathalie Teuber studies mathematics at the Technical University of Berlin with focus on differential geometry. Since 2005 she works as student assistant at the Scientific Visualization department of Zuse Institute Berlin (ZIB) in the area of visualization and feature extraction in flow fields.

Hans-Christian Hege is head of the Scientific Visualization department at Zuse Institute Berlin (ZIB). After studying physics and mathematics he performed research in computational physics and quantum field theory at Freie Universität Berlin (1984-89). Then he joined ZIB, initially as scientific consultant for high performance computing then as head of the Scientific Visualization department, which he started in 1991. His group performs research in data visualization and develops visualization software, like e.g. the Amira software. He is also co-founder of mental images (1986) and of Indeed - Visual Concepts GmbH (1999) which he built up as CEO (-2003) and which he now consults as scientific adviser. He regularly lectures at Universität Pompeu Fabra, Barcelona (Spain) and the German Film School (University for Digital Media Production) in Elstal, where he became honorary professor of Scientific Visualization in 2003. His current research interests are in visual data analysis and computer graphics as well as applications in engineering, natural and life sciences.